Study of the transition from self-organized to homogeneous plasma distribution in chromium HiPIMS discharge

M. Šlapanská[1], A. Hecimovic[2,*], J. T. Gudmundsson[3,4], J. Hnilica[1], W. Breilmann[2], P. Vašina[1], A. von Keudell[2]

[1] Department of Physical Electronics, Masaryk University, Kotlářská 2, CZ-61137, Brno, Czech Republic

[2] Institute for Experimental Physics II, Ruhr-University Bochum, D-44801 Bochum, Germany

[3] Department of Space and Plasma Physics, School of Electrical Engineering, KTH Royal Institute of Technology, SE-100 44, Stockholm, Sweden

[4] Science Institute, University of Iceland, Dunhaga 3, IS-107 Reykjavik, Iceland

∗ Max-Planck-Institute for Plasma Physics, Boltzmannstrasse 2, D-85748 Garching, Germany

E-mail: slapanska@physics.muni.cz

Abstract. The self-organised plasma patterns, known as spokes or ionisation zones in magnetron sputtering discharges, were observed in a wide range of power densities, from low power direct current magnetron sputtering (dcMS) discharge to high power impulse magnetron sputtering (HiPIMS) discharge. For some target materials and non-reactive gases, it was observed that at very high power densities (> 3 kW/cm^2) the plasma exhibits a transition from a regime where spokes are observed to a homogeneous plasma regime. In this contribution we present a comparison of plasma properties: plasma emission (optical emission spectroscopy) and flux of Ar^+ and Cr^+ ions (mass spectrometry), measured both in the spoke regime and in the homogeneous regime, aimed to expand the understanding of the plasma transition between the two modes. A simple biased flat probe was used to distinguish between the spoke regime and the homogeneous plasma regime. It was found that the flux of multiply charged ions (Ar^{2+}, Cr^{2+}, Cr^{3+}, Cr^{4+}) increases abruptly at the transition between spoke regime and homogeneous plasma regime. Similarly, the emission from Cr^+ ions exhibits a strong increase of about 50 % when the plasma torus becomes homogeneous. These observations are interpreted as an increase in electron temperature and change in the electron heating mode, from a combination of secondary electron heating and Ohmic heating towards pure Ohmic heating. The transition to homogeneous plasma and pure Ohmic heating is only observed in non-reactive HiPIMS discharges for target atoms with second ionisation potential higher than the first ionisation potential of Ar (15.76 eV), and a self-sputter yield larger than 1.

Submitted to: *Journal of Physics D: Applied Physics*

PACS numbers: 52.25.Xz, 52.70.Kz

1. Introduction

The magnetron sputtering method was developed during the sixties and seventies of the last century [1]. Sputtering is a physical process where target (cathode) atoms are knocked-out by incoming energetic ions of the working gas. A source of these ions is a plasma discharge, which is confined close to the cathode target by an external magnetic field. The magnetic field is not homogeneously distributed above the target, therefore, the plasma density is spatially inhomogeneous as well. In the region with a higher plasma density, a more intense sputtering of the cathode target occurs, creating the so-called racetrack [1]. An advanced method of magnetron sputtering is high power impulse magnetron sputtering (HiPIMS) [2, 3, 4]. In HiPIMS, the power is applied to the cathode target in pulses with a duration from several tens to hundreds of microseconds. The pulses are of high instantaneous power, whereas the average power remains comparable with the power used for direct current magnetron sputtering (dcMS), because a duty cycle is in percent range to protect the target from overheating. The discharge current densities in the pulse are usually several A$\cdot$cm^{-2}. This leads to a high ionization degree of the working gas atoms, intense sputtering and high ionization degree of the target atoms [5, 6, 7].

Recently, it was discovered that the plasma in a HiPIMS discharge is not always azimuthally homogeneously distributed above the racetrack, but under certain conditions, the plasma is self-organised into localised bunches [8], also called plasma instabilities [9], spokes [10] or ionization zones [11]. The spoke properties are highly dependent on the experimental conditions including the chamber geometry. It was found that spokes usually rotate in the $\mathbf{E}\times\mathbf{B}$ direction at the discharge currents of HiPIMS discharges [8, 9, 10], but at lower discharge currents typical for dcMS discharges the spokes were observed to move in the opposite direction [12, 13, 14]. The velocities of spokes rotating in the $\mathbf{E}\times\mathbf{B}$ direction are usually of about 10 km$\cdot$s^{-1}, i.e. 10 % of the electron drift velocity [8, 9, 10, 11, 15]. The spokes rotating in the reverse direction reach lower velocities, typically hundreds of m$\cdot$s^{-1} [12, 13]. Depending on the magnetic field strength and target material, various spoke shapes were detected [16, 17, 18, 19, 20]. They were categorised into several groups according to their shape: non-recognizable spokes, stochastic spokes, diffusive spokes, triangular spokes, and round spokes [21]. The spoke mode number increases with the magnetic field strength and it is also strongly dependent on discharge current and working gas pressure [17, 21, 22, 23]. Both, an increase [8, 21, 23, 24] as well as a decrease [15, 17, 19, 21, 22] of the spoke mode number with increasing the discharge current were observed depending on the particular experimental setup.

Using certain target materials, such as Cr, Cu, Mo or Ta with argon as the working gas, the so-called spoke-to-homogeneous transition was observed during the gradual increase of the discharge current [17, 19, 25, 26]. At lower discharge currents, the homogeneous plasma reorganises into localised spokes. As the discharge current increases, the spokes start merging, which results in the decrease of the spoke mode

number. Any further increase of the discharge current leads to spokes disappearance, and the plasma emission becomes azimuthally homogeneous [17]. The transition to a homogeneous plasma has not been observed in reactive HiPIMS [27]. When operating in the homogeneous regime, the plasma exhibits a high impedance and a low conductivity [17, 25]. Moreover, the ion flux towards the substrate together with the deposition rate increases in the homogeneous regime compared to the spoke regime [25]. Breilmann et al. [19] showed that during the transition from spoke regime to the homogeneous regime the high energy part of the ion energy distribution function (IEDF) is not affected and only the low energy part is modified.

The aim of this work is to expand the understanding of the plasma transition from self-organised spokes into homogeneously distributed plasma, by observing the change in plasma emission and in flux of Ar^+ and Cr^+ ions. A simple biased flat probe was used to distinguish between the spoke regime and the homogeneous plasma regime. The change in emission from Ar and Cr atoms and Cr^+ ions between the two regimes was measured using time-resolved optical emission spectroscopy (OES). Furthermore, the temporal evolution of Ar^+, Ar^{2+} and Cr^+, Cr^{2+}, Cr^{3+}, Cr^{4+} ion fluxes were monitored by time-resolved ion mass spectrometry (MS).

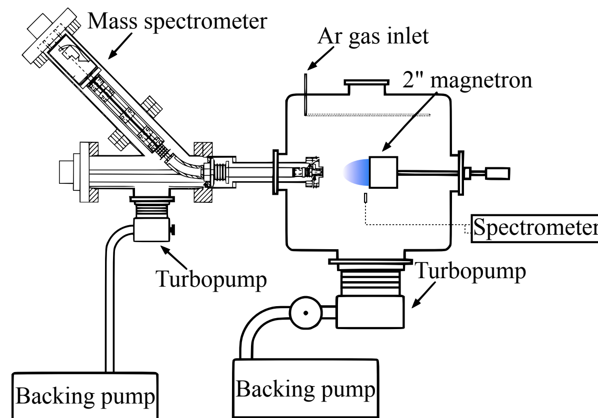

Figure 1. Simplified scheme of the side view of the experimental setup.

2. Experimental setup

The experiments were carried out using a low-pressure magnetron sputtering system adapted for plasma diagnostics. A schematic of the experimental setup is shown in Figure 1. The cylindrical vacuum chamber with dimensions of 35 cm in diameter and 45 cm in height was equipped with a two-stage vacuum system. The turbomolecular pump Pfeiffer TMU 1601 was backed up by secondary pump Pfeiffer Vacuum DUO 035 and reached a base pressure of $8{\times}10^{-4}$ Pa. The pressure was measured by a capacitive Oerlikon Leybold Vacuum CTR 101 pressure gauge. The working gas pressure of 0.5 Pa was set by a mass flow controller Aera FC-DR980.

The 2-inch chromium target (3 mm thickness) was fitted to an unbalanced circular planar magnetron assembly, which served as a sputter source. The discharge was driven by a TruPlasma Highpulse 4002 generator manufactured by Hüttinger Electronik capable of supplying a maximum voltage of 2 kV and a maximum current of 1 kA within a pulse. The pulse length was set to 200 µs with a repetition rate of 10 Hz providing a duty cycle of 0.2 %. The waveforms were recorded by an oscilloscope Tektronix TPS 2024.

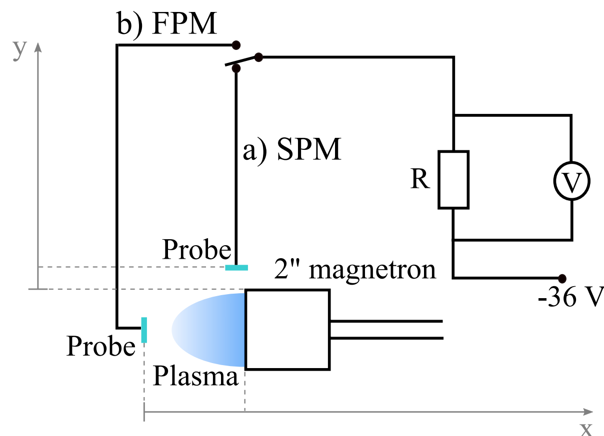

Figure 2. Simplified scheme of the experimental setup for the probe measurements.

Figure 2 shows the simplified scheme for the probe measurements. The probe was biased by -36 V, which attracted the ions and repelled the electrons. The ion saturation current, probe current, was determined by measuring the voltage drop over a resistor placed in series with the biasing circuit. A rectangular flat probe (10 mm×5 mm) was mounted in two configurations: (a) side probe measurements (SPM) and (b) face probe measurements (FPM). In the case of SPM, the probe was mounted next to the target edge, i.e., perpendicular to the target surface. The probe could be moved away from the target along the y-axis, as shown in Figure 2. The zero position was at the edge of the target. For SPM, the probe current was determined by measuring the voltage across a 100 Ω resistor. In the case of FPM, the probe was placed facing the centre of the circular target. The whole magnetron assembly could be moved away from the probe along the x-axis direction, as shown in Figure 2. In FPM, a zero position of the probe was at the surface of the target, but the closest measuring distance was 3 cm above the target surface. In FPM, a resistor of 6.8 Ω was employed due to higher ion flux to the probe in comparison with SPM. In both configurations, the probe was placed at six positions with a step of 1 cm, i.e., the SPM was placed between 0 and 5 cm from the target edge and the FPM between 3 and 8 cm from the target surface.

The time-resolved OES was carried out using the two channels USB spectrometer Avantes AvaSpec-ULS2048XL. The spectrometer covers the spectral range of 200 – 1100 nm with 0.75 nm resolution. Optical fibre with collimator was placed into the holder in the chamber to collect the light 2 mm above the target surface. The

	λ (nm)	A_{ki} (s^{-1})	E_i (eV)	E_k (eV)	Lower Level	Upper Level
Ar I	763.51	2.45e+07	11.54835	13.17178	$3s^2 3p^5(^2P_{3/2})4s$	$3s^2 3p^5(^2P_{3/2})4p$
Cr I	425.44	3.15e+07	0.00000	2.91348	$3d^5(^6S)4s$	$3d^5(^6S)4p$
Cr II	267.18	1.0e+08	1.50613	6.14522	$3d^4(^5D)4s$	$3d^4(^5D)4p$

Table 1. Wavelength (λ), Einstein coefficients of spontaneous emission (A_{ki}), energy of lower (E_i) and upper (E_k) spectral state and spectral transition [28].

investigated spectral lines of Ar I, Cr I and Cr II and some relevant parameters are described in Table 1.

The time-resolved ion flux of Cr^+, Cr^{2+}, Cr^{3+}, Cr^{4+}, Ar^+ and Ar^{2+} was measured a using HIDEN EQP 300 HE mass spectrometer. The target and the mass spectrometer faced each other at a distance of 5 cm. The mass spectrometer orifice (50 µm in diameter) was tilted by 3° to point at the racetrack of the target. The temporal resolution was 2 µs. The time axis compensation was performed for each ion by calculating the time-of-flight through the mass spectrometer. A more detailed description of the MS setup is given elsewhere [19].

3. Results

3.1. Spoke detection in an argon/chromium HiPIMS discharge by flat probe

The presence or absence of spokes in the discharge is determined using the flat probe. Breilmann et al. [19] showed that the regular peaks observed on the signal from the flat probe in SPM correspond to the passing spokes and the occurrence of a constant signal indicates a homogeneous plasma distribution along the torus.

In this study, the flat probe was placed next to the target edge to perform the side probe measurements (SPM), as illustrated in Figure 2. The typical flat probe signals acquired at the position $y = 2$ cm from the target edge are shown in Figure 3(b), and the corresponding discharge current waveforms are shown in Figure 3(a). All flat probe signals increase from the beginning of the pulse until 125 µs, similar to the discharge current. The peaks on all three probe signals indicate the appearance of stochastic spokes roughly after 45 µs.

The transition from the spoke regime to homogeneous distribution during the HiPIMS pulse occurs the time interval from 125 µs to 200 µs. This region of interest is marked by grey dashed lines in figures throughout this paper. Long pulses (200 µs) were chosen in order to allow the discharge to evolve and to reach the most stable plasma conditions, where the discharge current reached a plateau.

Three current levels of discharge are chosen. At the lowest discharge current, **Pulse I**, the plasma is in the spoke regime after 125 μs. The peaks in the probe signal are observable until the end of Pulse I where the discharge current during the plateau is ~ 50 A and the cathode voltage is about -740 V. The plasma parameters of **Pulse II** are adjusted to reach the so-called transition regime. For Pulse II, the discharge current

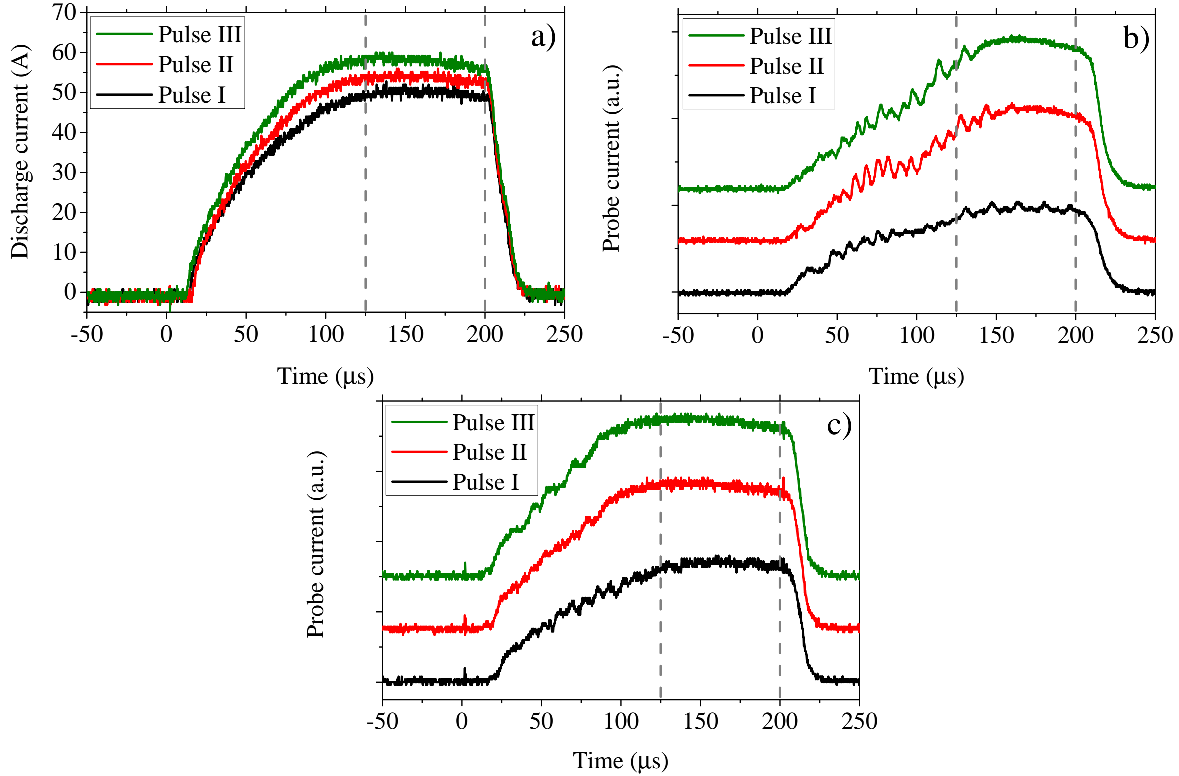

Figure 3. (a) Discharge current waveforms for Pulses I, II and III. (b) The flat probe signals for Pulses I, II and III in **side probe measurements** (SPM) with the flat probe placed 2 cm from the target edge. (c) The flat probe signals for Pulses I, II and III in **face probe measurements** (FPM). The flat probe was placed 3 cm from the target centre. The argon pressure was 0.5 Pa.

is $\sim$ 54 A and the cathode voltage is about -760 V, the peaks are visible only until 165 µs into the pulse. At later times during the pulse, a constant signal is detected. The transition from spoke regime to homogeneous plasma distribution occurs during the time window when the discharge is constant. And at the highest current, **Pulse III**, the plasma reaches the homogeneous regime. A constant signal and thus a homogeneous plasma distribution is observed after 125 µs until the pulse to the end of Pulse III with a discharge current of $\sim$ 57 A and a cathode voltage of about -780 V. The plasma appearance is classified at its steady state when the plateau region in current waveform is reached, for better clarity see Table 2.

For the face probe measurements (FPM), the probe faced the centre of the circular target, as illustrated in Figure 2. Figure 3(c) shows the flat probe signals for Pulses I, II and III for the probe at position $x = 3$ cm. The flat probe signals show no peaks in the plateau region for all three HiPIMS pulses, even in the case of Pulse I where the plasma exhibits spokes, as it was shown by the previous side probe measurements. The flat probe in FPM captures the signal generated by the whole plasma, because it is placed above the geometrical centre of the target. Due to the symmetry, it is impossible to observe a modulation on the probe signal, although one or more spokes may rotate.

Similar probe signal evolutions were acquired for the flat probe at positions $3 - 8$ cm apart from the target. Therefore, only SPM can be used for reliable spoke detection.

Figure 4 shows the flat probe signal for Pulse I for various positions of the flat probe $y = 0 - 5$ cm. The peaks indicating presence of spokes are clearly visible even for the farthest flat probe position at 5 cm.

Name	Plateau discharge current (A)	Cathode voltage (V)	Observed plasma distribution
Pulse I	~ 50 A	-740 V	spoke regime
Pulse II	~ 54 A	-760 V	spoke-homogeneous transition
Pulse III	~ 57 A	-780 V	homogeneous plasma regime

Table 2. Overview of investigated experimental conditions and observed plasma distribution for time interval from 125 µs to 200 µs in side probe measurements (SPM). The flat probe was placed at 2 cm from the target edge. The argon pressure was 0.5 Pa.

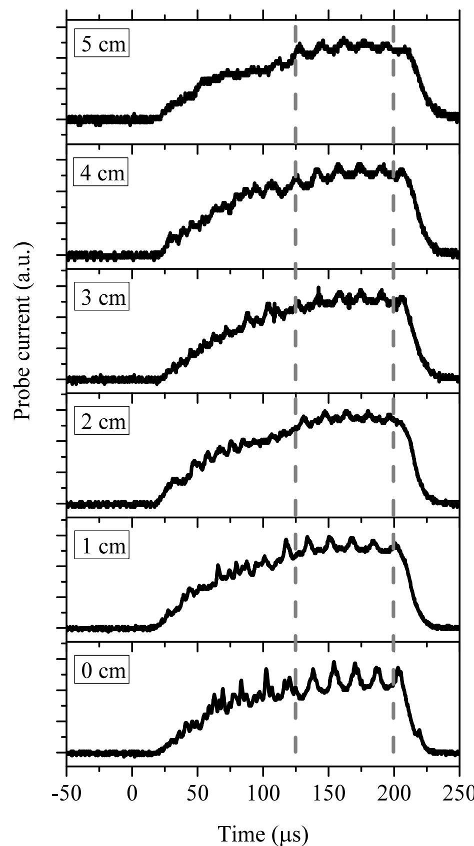

Figure 4. Flat probe currents for Pulse I in SPM for various flat probe positions. The argon pressure was 0.5 Pa.

3.2. Optical emission spectroscopy measurements

Overview spectra, as well as the temporal evolution of selected spectral lines intensities obtained by OES for Pulses I, II and III were investigated. The overview optical emission spectra are shown in Figure 5 only for Pulses I and III. The overview spectrum of Pulse II is not shown here, because it is very similar to the spectrum obtained for Pulse I. The overview spectra were recorded in the range of 225 – 950 nm at 170 μs into the pulse, where stable plasma conditions were reached. It can be seen that the most intense spectral lines are Cr I lines (around 357, 427, 520, 693 and 740 nm) and Cr II lines (265 – 345 nm). The argon atom lines are approximately 100× weaker indicating either Ar rarefaction or substantial Ar ionisation [29, 30, 31, 32]. The intensities of the Cr I lines in the overview spectrum recorded for Pulse III are slightly higher compared to the case of Pulse I. However, the intensities of Cr II lines are significantly higher for Pulse III, i.e., for homogeneous plasma distribution, despite the discharge current being only ∼ 14 % higher compared to Pulse I in this case.

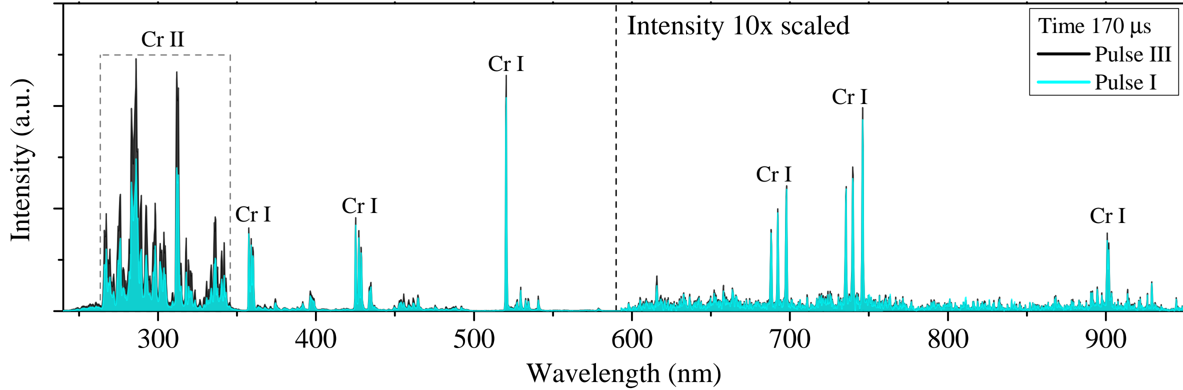

Figure 5. Overview emission spectra of the argon/chromium HiPIMS discharge at 170 μs for Pulses I and III. The argon pressure was 0.5 Pa.

The temporal evolution of Ar I (763.51 nm), Cr I (425.44 nm) and Cr II (267.18 nm) line intensities during all three HiPIMS pulses are shown in Figures 6(a),(b) and (c), respectively. The evolution of the Ar I line intensity reveals a pronounced peak, as shown in Figure 6(a). The intensity of the Ar I line sharply increases during the first 27 μs of the HiPIMS pulse and reaches a maximum. Afterwards, it decreases very quickly due to the gas rarefaction [29, 30, 31, 32, 33]. The same evolution of the Ar I line intensity is observed for all three pulses. The time-resolved evolutions of the Cr I line intensities to a large extent follow the discharge current. The intensity of the Cr I line increases by 9 % for Pulses II and III in comparison to Pulse I, as shown in Figure 6(b). For Pulses I and II, the intensity is almost the same, but for Pulse III the Cr II line intensity increases by roughly 50 %, as shown in Figure 6(c).

The OES data shown strong emission of chromium ions in the overview spectra as was expected. Moreover, it revealed that the Cr II line intensity increases about 50 % for Pulse III compared to Pulse I, while the discharge current increased only slightly.

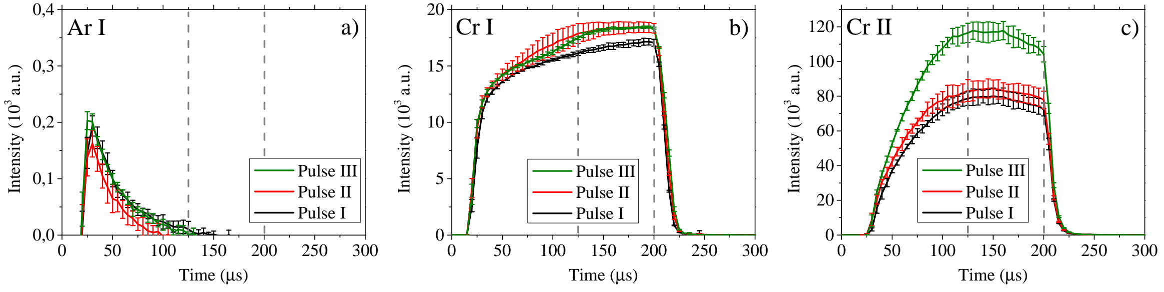

Figure 6. Time-resolved evolution of the (a) Ar I (763.51 nm), (b) Cr I (425.44 nm) and (c) Cr II (267.18 nm) lines emitted from argon/chromium HiPIMS plasma for Pulses I, II and III. The argon pressure was 0.5 Pa.

3.3. Time-resolved ion fluxes

The mass spectrometer was used to measure the time-resolved evolution of the ion fluxes of Ar^{+}, Ar^{2+}, Cr^{+}, Cr^{2+}, Cr^{3+} and Cr^{4+}. The ion flux was obtained by integrating the ion energy distribution function (IEDF). The detector was mounted at a distance of 5 cm from the target. The time dependence of ion fluxes of Ar^{+} and Ar^{2+} are shown in Figures 7(a) and (b), respectively. The Ar^{+} ion flux exhibits a similar time dependence for all three HiPIMS pulses. The Ar^{+} ion flux sharply increases during the first 60 µs of the HiPIMS pulse, reaches a maximum and gradually decreases afterwards. Nevertheless, if the linear scale is used (see Figure 7(a)), the Ar^{+} ion flux is the highest for Pulse I while the lowest for Pulse III from the beginning of the pulse until 150 µs. Then the Ar^{+} ion flux for Pulses I and II decreased faster and the Ar^{+} ion flux is the highest for Pulse III and the lowest for Pulse I till the end of the pulse. A similar evolutions are also observed for the Ar^{2+} ion flux. However, the change occurs earlier (at 100 µs) and the Ar^{2+} ion flux increases and then saturates for Pulses II and III, while for Pulse I it still gradually decreases. The Ar^{2+} ion flux is higher by a factor of 2.3 for Pulse III compared to Pulse I at the time of 170 µs, while the discharge current increased only by about 14 %.

One could expect that the Ar^{+} ion count is reduced when the discharge current is increased due to the transition to self-sputtering [34]. As described by Huo et al. [31], the results from an ionization region model (IRM) suggested that at pressures lower than 1.8 Pa (the pressure at which they ran their model) the density of Ar atoms that are trapped in the target surface, and eventually become sputtered (warm recombined Ar) could be larger than the density of background Ar atoms (cold Ar). Therefore, an observed increase of Ar^{2+} ions in the homogeneous regime, shown in Figure 7(b), could originate from recombined Ar^{+} ions that return from the target as neutrals and were ionised in the target vicinity.

Figure 7(c) shows the temporal evolution of the Cr^{+} ion flux. The highest flux of Cr^{+} ions is detected for Pulse III and the lowest ion flux for Pulse I during the whole HiPIMS pulse. Similarly to the Ar^{2+} ions case, the increase of Cr^{2+}, Cr^{3+} and Cr^{4+} ion fluxes are observed at 100 µs for Pulses II and III, and shown in Figures 7(d),(e) and (f),

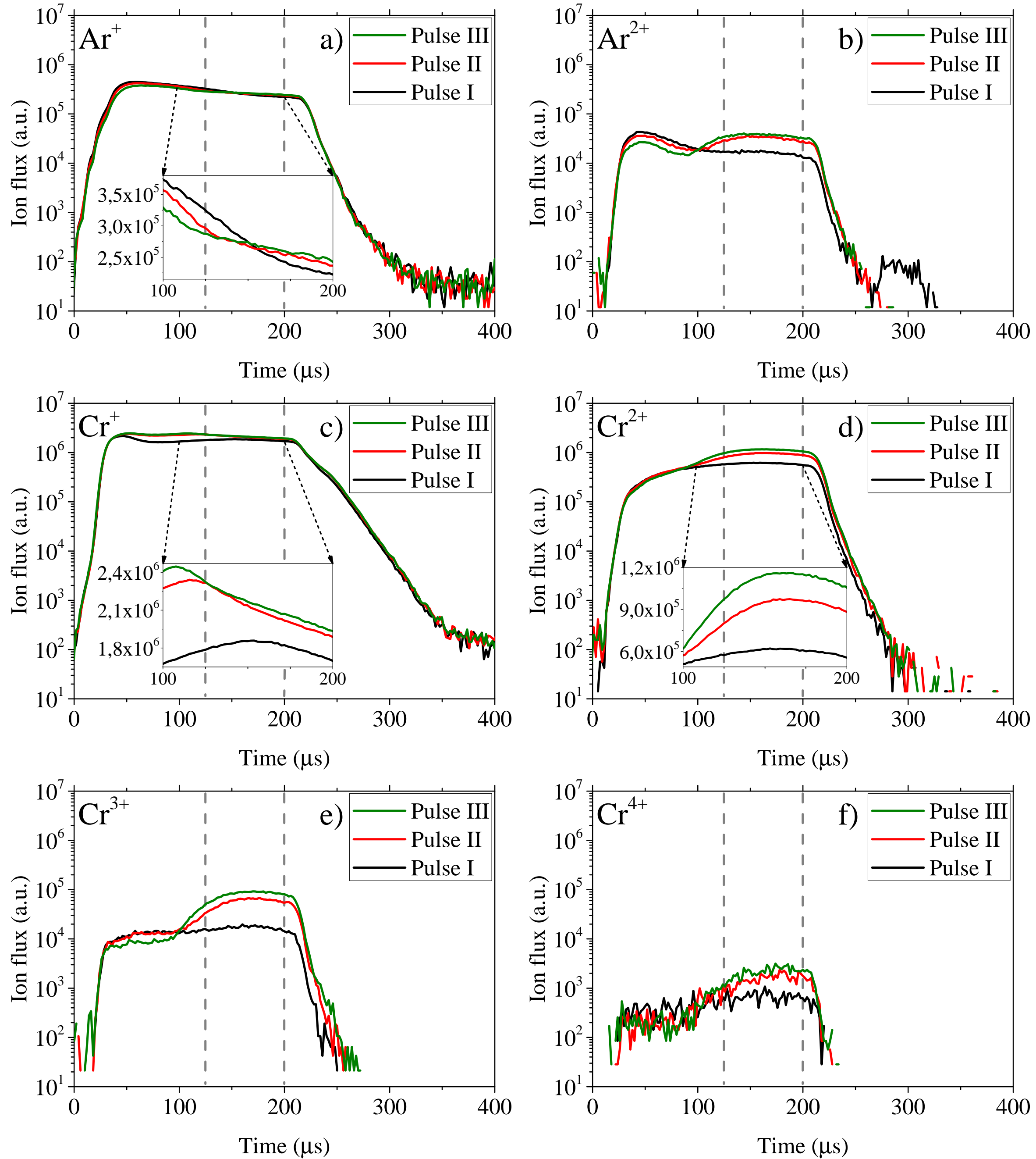

Figure 7. The relative ion fluxes of Ar^+, Ar^{2+}, Cr^+, Cr^{2+}, Cr^{3+} and Cr^{4+} from the argon/chromium HiPIMS plasma as a function of time after pulse ignition. The distance between the mass spectrometer orifice and the target was 5 cm and the argon pressure was 0.5 Pa.

respectively. Comparing Pulse III and Pulse I at 170 µs, the ion flux of Cr^{2+} increases by a factor of 1.9, the ion flux of Cr^{3+} even by a factor of 5 and Cr^{4+} ion flux increases by a factor of 2.3. In Table 3, the relative ion fluxes for Pulses I and III at 170 µs are shown. In conclusion, the homogeneously distributed plasma generates a significantly higher flux of multiply charged ions at the distance of 5 cm such as Ar^{2+}, Cr^{2+}, Cr^{3+}

and Cr^{4+} compared to the plasma with a pronounced spoke pattern.

	Ar^{+}	Ar^{2+}	Cr^{+}	Cr^{2+}	Cr^{3+}	Cr^{4+}
Pulse I	8.98 %	0.62 %	67.07 %	22.62 %	0.68 %	0.03 %
Pulse III	7.21 %	1.04 %	57.29 %	31.86 %	2.55 %	0.05 %

Table 3. The relative ion flux composition of Ar^{+}, Ar^{2+}, Cr^{+}, Cr^{2+}, Cr^{3+} and Cr^{4+} from argon/chromium HiPIMS plasma at 170 µs for Pulses I and III corresponding to spoke regime and homogeneous regime, respectively. The argon pressure was 0.5 Pa.

4. Discussion

From the experiments one can see that a relatively small change in the applied power density (from 1.9 kW/cm^2 to 2.2 kW/cm^2, corresponding to change in the cathode voltage from 740 V to 780 V) causes a transition from spoke regime to homogeneous regime, characterized by a strong increase in ion production as shown by optical emission spectroscopy and ion mass spectrometry measurements. Furthermore, an increase in the ion flux of highly charged ions indicates an increase in electron temperature. Here, we assume that the dominant excitation and ionisation mechanism of atoms and ions is electron-impact excitation and ionisation at the pressure of our experiment. The ionisation energies of the relevant species are shown in Table 4.

	E_{iz} (eV)		E_{iz} (eV)
Cr^{+}	6.76	Ar^{+}	15.76
Cr^{2+}	16.48	Ar^{2+}	27.63
Cr^{3+}	30.96		
Cr^{4+}	49.16		

Table 4. Ionisation energy of the observed ions [28].

There are two mechanisms that provide energy for the electrons in the sheath and pre-sheath region near the target, respectively. The first mechanism is the acceleration of the secondary electrons in the cathode sheath emitted from the target surface (**sheath energisation**). The second mechanism is **Ohmic heating**, suggested by Huo et al. [35] based on calculations by an ionization region model (IRM) [36], where electrons gain energy in the cathode pre-sheath by dissipation of locally deposited energy $\mathbf{j} \cdot \mathbf{E}$ to the species in the pre-sheath region. Huo et al. [35] have shown that in HiPIMS discharges using target materials with high second ionisation potential, like Al and Cr, the dominating energy transfer mechanism to the electrons is through Ohmic heating. The reasoning is that for high power HiPIMS plasma, the Ar gas is strongly depleted, and metal ions are the dominant ion species. Since Al^{+} (and Cr^{+}) ions have a secondary electron yield of ~ 0 when bombarding the target of the same element [37], the plasma can only be sustained by electrons gaining energy from Ohmic heating.

Brenning et al. [38] expanded on the Ohmic theory in dcMS discharges and found that Ohmic heating becomes the more important electron heating mechanism compared to the sheath energisation, because the secondary electron yield reduces from 0.1 towards 0, thus having the highest contribution to the total ionisation. The effectiveness of the transition to Ohmic heating will also depend on the self-sputter yield of the element as a larger self-sputter yield will enhance Ar rarefaction.

According to the literature, it is possible to recognise two groups of plasmas regarding their appearance at high power densities (above several kW/cm^2); *Group 1* plasmas exhibit transition to homogeneous regime at high powers, and *Group 2* plasmas that at high powers exhibit spokes with diffuse shape [39]. The *Group 1* comprises of plasmas generated in the following material/gas combination: in Ar gas: Al, Au, Cr, Cu, Mo and Ta, in Kr gas: Al, and in the gasless environment: Cu. The common features of these materials are: the second ionisation potential is higher than the first ionisation potential of Ar (15.76 eV), and the self-sputter yield is larger than 1, $Y_{ss} > 1$. It is characteristic to exhibit a triangular spoke shape before the transition to homogeneous regime [12, 16, 40] for all these materials.

The plasmas in *Group 2* do not exhibit a transition to homogeneous regime and this has been observed for target materials with the second ionisation potential lower than the first ionisation potential of Ar (15.76 eV) [9, 15, 16, 20, 21, 22, 23] and self-sputter yield lower than 1 ($Y_{ss} < 1$), such as Ti and Nb. The reactive HiPIMS discharges (Al/N_2, Al/O_2, Cr/N_2, Cr/O_2, Ti/N_2, Ti/O_2) [27] also belong to *Group 2*. These discharges are characterised by a high density of doubly charged ions, and a compound layer on the cathode target during reactive HiPIMS, which can be correlated to secondary electron yield higher than that during a pure Ar discharge [16, 41]. Additionally, for both HiPIMS plasmas using Ti and Nb targets, and for reactive HiPIMS, it is characteristic to observe a transition from triangular spoke shape to diffuse spoke shape at higher power densities [12, 16, 40].

Figure 8 shows a visual representation of *Group 1* and *Group 2*. There, the target materials are plotted as a function of the self-sputter yield (Y_{ss}) and the ratio of the second ionisation potential of the target element ($E^{M}_{iz,2}$) to the first ionisation potential of Ar ($E^{Ar}_{iz,1}$). The self-sputter yield values are calculated at highest achievable voltages before the discharge becomes unstable, typically due to arcing. Blue colour represents elements from *Group 1*, and red colour represents elements from *Group 2*. In reactive HiPIMS, the self-sputter yield is low [42] and the ionisation potential of reactive gas atoms (N at 14.53 eV, and O at 13.61 eV) is lower than that of Ar, therefore belonging to *Group 2*.

The transition from the spoke regime to the homogeneous regime, leads to an increase in the ion emission and the ion flux of highly charged ions, that appears when the cathode voltage is increased by only 5 % (from 740 V to 780 V). Such a strong increase in the ion species signal cannot be explained only by an increase in the high energy tail of EEDF. An increase of the cathode voltage will surely affect the high energy tail of the EEDF through the acceleration of the secondary electrons from the target in

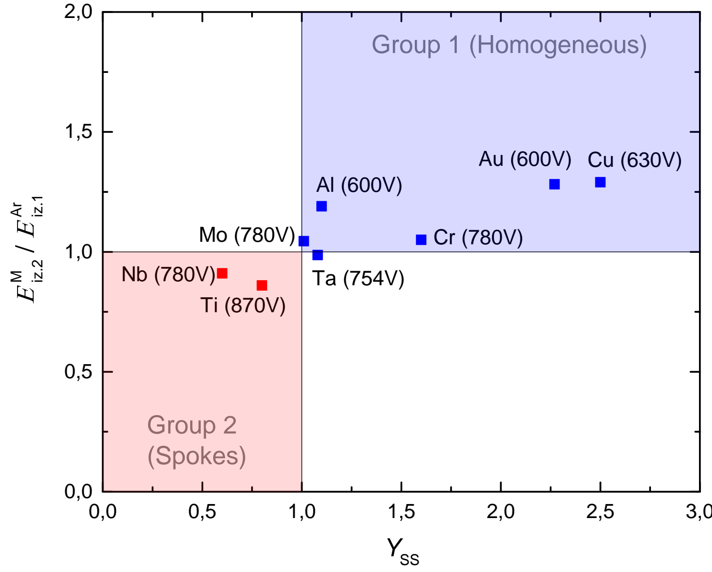

Figure 8. Different target materials plotted as a function of self-sputter yield (Y_{ss}) and the ratio of the second ionisation potential of the element ($E^{M}_{iz,2}$) to the first ionisation potential of Ar ($E^{Ar}_{iz,1}$). The voltages in brackets represent the value at which the self-sputter yield values are calculated.

the cathode sheath, but this can only be a minor effect.

Our hypothesis is that in spoke regime, electron heating is a combination of secondary electron acceleration and Ohmic heating. The location of highly charged ions in the spoke [43] and the localisation of the discharge current in the spokes [44, 45] indicate, that energetic secondary electrons are "defining" the ionisation region. It has been shown that the discharge current to the target is never 0 between the spokes, which means that Ohmic heating between the spokes is probably present, and within the spokes it is enhanced by the secondary electrons [44, 45].

In the case of *Group 1* atoms, at certain power the Ar density drops (probably due to high sputter yield), the secondary electrons emission will diminish, and all power input into the discharge will be delivered through Ohmic heating process. This will eventually lead to a higher electron temperature overall, not just within the spokes and to a more homogeneous sputtering with more sputtered material produced (as shown in the work of de los Arcos et al. [25]).

The transition to solely Ohmic heating is probably triggered by an increase in the electron density above a certain threshold where the increase in the power cannot be sustained by secondary electrons as the density of Ar^{+} and Ar^{2+} ions is reduced by rarefaction (for example see the negative slopes observed for Ar^{+} ions in Figures 7(a) and (b) between 50 to 125 μs). Furthermore, the density of the multiple charged metal ions is not sufficiently high to compensate for the lack of secondary electrons. The transition to the homogeneous regime is more probable to occur for elements with sputter yields higher than 1 (more efficient Ar rarefaction), and high secondary ionisation potential (lower doubly charged ion density), which is a characteristic of elements belonging to

Group 1.

This interpretation is corroborated by the analysis of the discharge current contributions using the IRM model. The discharge current contributions of a non-reactive HiPIMS discharge with Al (1.8 Pa) and Ti (0.54 Pa) target are compared [46]: for Al target it was found that at 360 V ($E_p < 0.1$ J) and 400 V ($E_p = 0.5$ J), there is significant contribution of Ar^+ ions to the discharge current, while at 800 V ($E_p =$ 6.4 J), the discharge current is predominantly composed of Al^+ ions. According to Poolcharuansin et al. [44], a HiPIMS discharge with Al target at 1.8 Pa and above E_p = 2 J is in the homogeneous regime, which is consistent with our explanation for the elements from *Group 1*. The discharge current contributions of the HiPIMS discharge with a Ti target comprised of Ar^+, Ti^+, and Ti^{2+} ions, in descending order. Bohlmark et al. [47] reported on up to a 24 % contribution of Ti^{2+} ions in HiPIMS with Ti target. This is consistent with our explanation for the elements from *Group 2*, where the spokes are present at high power densities.

In reactive HiPIMS discharges (also belonging to *Group 2*) with Ti target and Ar/O_2 background gas mixture, it was shown that in the metal mode Ar^+ and Ti^+ ions are the main discharge current contributions at the target surface, while in the poisoned mode the Ar^+ ions contributes to more than 80 % of the total discharge current [42]. Due to the high Ar^+ ion contribution to the discharge current, there are more secondary electrons contributing to the electron heating, while the self-sputter yield of Ti^+ ion is below unity, reactive HiPIMS discharge fits well to the requirements of the *Group 2*. In reactive HiPIMS, the transition to a homogeneous discharge has not been observed [27].

For the plasma, driven by Ohmic heating, more highly ionized particles will be produced, simply because Ohmic heating occurs over the whole racetrack area, while for the secondary electron driven plasma, the ionisation tends to be very localized [43]. Huo et al. [35] estimated that the potential drop in the pre-sheath is of the order of 100 V, which is sufficiently high to energise electrons to produce highly charge chromium ions observed in this work. As the ions are ionised in the pre-sheath volume, it is possible that their kinetic energy is sufficient to leave the pre-sheath region and reach the orifice of the mass spectrometer, rather than to be back-attracted to the cathode target.

Assuming that the targets can be cooled sufficiently, it is possible that the homogeneous plasma mode can be reached for all materials above a certain electron density. The ways and thresholds to reach such a high plasma density might be, however, different and challenging depending on the target material. For example, materials with a high self sputter yield allow more easily to reach high plasma density. The same might be true for the cases of low self sputter yield material, where at certain material specific threshold the Ohmic heating in the pre-sheath becomes significant.

5. Conclusions

The transition of the plasma pattern from spokes into the homogeneously distributed plasma in an argon/chromium HiPIMS discharge was studied by a flat probe, optical

emission spectroscopy and ion mass spectrometry. The flat probe was utilized to detect the presence of spokes in the discharge. A sufficient signal to verify the presence of spokes was detected up to 5 cm a distance of the side of the target. In the conditions where the plasma undergoes the transition from self-organized spokes towards the homogeneous plasma distribution, the strong 50 % increase of Cr II emission was observed together with a significant increase in the fluxes of multiply ionized species. The change from the self-organized spokes towards homogeneous plasma emission was explained to originate from an increase in electron temperature and change in the electron heating mode, from a combination of secondary electron heating and Ohmic heating towards pure Ohmic heating. The transition to a homogeneous plasma and pure Ohmic heating is only observed in non-reactive HiPIMS discharges for target atoms with second ionisation potential higher than the first ionisation potential of Ar (15.76 eV), and a self-sputter yield larger than 1, $Y_{ss} > 1$.

Acknowledgements

This research has been partially financially supported by the project LO1411 (NPU I) funded by Ministry of Education Youth and Sports of Czech Republic, the project CZ.1.05/2.1.00/03.0086 funded by European Regional Development Fund and project GA19-00579S funded by the Czech Science Foundation. This work has been supported by the German Science Foundation (DFG) within the frame of the collaborative research centre SFB-TR 87. The authors would like to thank Peter Klein and Julian Held for fruitful discussions.

References

[1] Powell R A and Rossnagel S M 1998 *PVD for Microelectronics: Sputter Deposition Applied to Semiconductor Manufacturing (Thin Films)* vol 26 (New York: Academic Press)
[2] Mozgrin D V, Fetisov I K and Khodachenko G V 1995 *Plasma Physics Reports* **21** 400–409
[3] Fetisov I K, Filippov A A, Khodachenko G V, Mozgrin D V and Pisarev A A 1999 *Vacuum* **53** 133–136
[4] Kouznetsov V, Macák K, Schneider J M, Helmersson U and Petrov I 1999 *Surface and Coatings Technology* **122** 290–293
[5] Gudmundsson J, Brenning N, Lundin D and Helmersson U 2012 *Journal of Vacuum Science & Technology A: Vacuum, Surfaces, and Films* **30** 030801
[6] Britun N, Minea T, Konstantinidis S and Snyders R 2014 *Journal of Physics D: Applied Physics* **47** 224001
[7] Biskup B, Maszl C, Breilmann W, Held J, Bke M, Benedikt J and von Keudell A 2018 *Journal of Physics D: Applied Physics* **51** 115201
[8] Kozyrev A V, Sochugov N S, Oskomov K V, Zakharov A N and Odivanova A N 2011 *Plasma Physics Reports* **37** 667–673
[9] Ehiasarian A P, Hecimovic A, de los Arcos T, New R, Schulz-Von Der Gathen V, Böke M and Winter J 2012 *Applied Physics Letters* **100** 114101
[10] Anders A, Ni P and Rauch A 2012 *Journal of Applied Physics* **111** 053304
[11] Anders A 2012 *Applied Physics Letters* **100** 224104
[12] Yang Y, Liu J, Liu L and Anders A 2014 *Applied Physics Letters* **105** 254101

[13] Hecimovic A, Maszl C, Schulz-von der Gathen V, Böke M and von Keudell A 2016 *Plasma Sources Science and Technology* **25** 035001

[14] Anders A and Yang Y 2018 *Journal of Applied Physics* **123** 043302

[15] Winter J, Hecimovic A, de los Arcos T, Böke M and Schulz-Von Der Gathen V 2013 *J. Phys. D: Appl. Phys.* **46** 084007

[16] Hecimovic A, Böke M and Winter J 2014 *J. Phys. D: Appl. Phys.* **47** 102003

[17] de los Arcos T, Layes V, Gonzalvo Y A, Schulz-von der Gathen V, Hecimovic A and Winter J 2013 *J. Phys. D: Appl. Phys.* **46** 335201

[18] Poolcharuansin P, Estrin F L and Bradley J W 2015 *Journal of Applied Physics* **117** 163304

[19] Breilmann W, Eitrich A, Maszl C, Hecimovic A, Layes V, Benedikt J and von Keudell A 2015 *J. Phys. D: Appl. Phys.s* **48** 295202

[20] Klein P, Lockwood Estrin F, Hnilica J, Vašina P and Bradley J W 2017 *Journal of Physics D: Applied Physics* **50** 015209

[21] Hnilica J, Klein P, Šlapanská M, Fekete M and Vašina P 2018 *Journal of Physics D: Applied Physics* **51** 095204

[22] Hecimovic A, Schulz-von der Gathen V, Böke M, von Keudell A and Winter J 2015 *Plasma Sources Science and Technology* **24** 045005

[23] Klein P, Hnilica J, Zemánek M, Bradley J W and Vašina P 2019 *Journal of Physics D: Applied Physics* **52** 125201

[24] Klein P, Hnilica J, Hubička Z, Čada M, Šlapanská M, Zemánek M and Vašina P 2017 *Plasma Sources Science and Technology* **26** 055015

[25] de los Arcos T, Schröder R, Gonzalvo Y A, Schulz-von der Gathen V and Winter J 2014 *Plasma Sources Science and Technology* **23** 054008

[26] von Keudell A, Hecimovic A and Maszl C 2016 *Contributions to Plasma Physics* **56** 918–926

[27] Hecimovic A, Corbella C, Maszl C, Breilmann W and von Keudell A 2017 *Journal of Applied Physics* **121** 171915

[28] Kramida A, Ralchenko Y, Reader J and Team N A Nist atomic spectra database (version 5.4) URL `https://physics.nist.gov/PhysRefData/ASD/lines_form.html`

[29] Vlček J, Pajdarová A and Musil J 2004 *Contributions to Plasma Physics* **44** 426–436

[30] Kadlec S 2007 *Plasma Processes and Polymers* **4** S419–S423

[31] Huo C, Raadu M A, Lundin D, Gudmundsson J T, Anders A and Brenning N 2012 *Plasma Sources Science and Technology* **21** 045004

[32] Kozák T and Lazar J 2018 *Plasma Sources Science and Technology* **27** 115012

[33] Vitelaru C, Lundin D, Stancu G D, Brenning N, Bretagne J and Minea T 2012 *Plasma Sources Science and Technology* **21** 025010

[34] Anders A 2011 *Surface and Coatings Technology* **205** S1–S9

[35] Huo C, Lundin D, Raadu M A, Anders A, Gudmundsson J T and Brenning N 2013 *Plasma Sources Science and Technology* **22** 045005

[36] Raadu M A, Axnäs I, Gudmundsson J T, Huo C and Brenning N 2011 *Plasma Sources Science and Technology* **20** 065007

[37] Anders A 2008 *Applied Physics Letters* **92** 201501

[38] Brenning N, Gudmundsson J T, Lundin D, Minea T, Raadu M A and Helmersson U 2016 *Plasma Sources Science and Technology* **25** 065024

[39] Hecimovic A and von Keudell A 2018 *Journal of Physics D: Applied Physics* **51** 453001

[40] Andersson J, Ni P and Anders A 2014 *IEEE Transactions on Plasma Science* **42** 2856–2857

[41] Corbella C, Marcak A, de los Arcos T and von Keudell A 2016 *Journal of Physics D: Applied Physics* **49** 16LT01

[42] Gudmundsson J T, Lundin D, Brenning N, Raadu M A, Huo C and Minea T 2016 *Plasma Sources Science and Technology* **25** 065004

[43] Andersson J, Ni P and Anders A 2013 *Applied Physics Letters* **103** 054104

[44] Poolcharuansin P, Estrin F and Bradley J W 2015 *Journal of Applied Physics* **117** 163304

[45] Hecimovic A, Held J, Schulz-von der Gathen V, Breilmann W, Maszl C and von Keudell A 2017 *Journal of Physics D: Applied Physics* **50** 505204

[46] Huo C, Lundin D, Gudmundsson J T, Raadu M A, Bradley J W and Brenning N 2017 *Journal of Physics D: Applied Physics* **50** 354003

[47] Bohlmark J, Lattemann M, Gudmundsson J T, Ehiasarian A P, Gonzalvo Y A, Brenning N and Helmersson U 2006 *Thin Solid Films* **515** 1522–1526